

# Peri-Decoration of a Tetraazaperylene with Urea Units: Chiral Octaazaperopyrenedioxides (OAPPDOs) and Their Optical and Chiroptical Properties

Tobias Wesp,<sup>[a]</sup> Tim Bruckhoff,<sup>[a]</sup> Hubert Wadepohl,<sup>[a]</sup> and Lutz H. Gade\*<sup>[a]</sup>

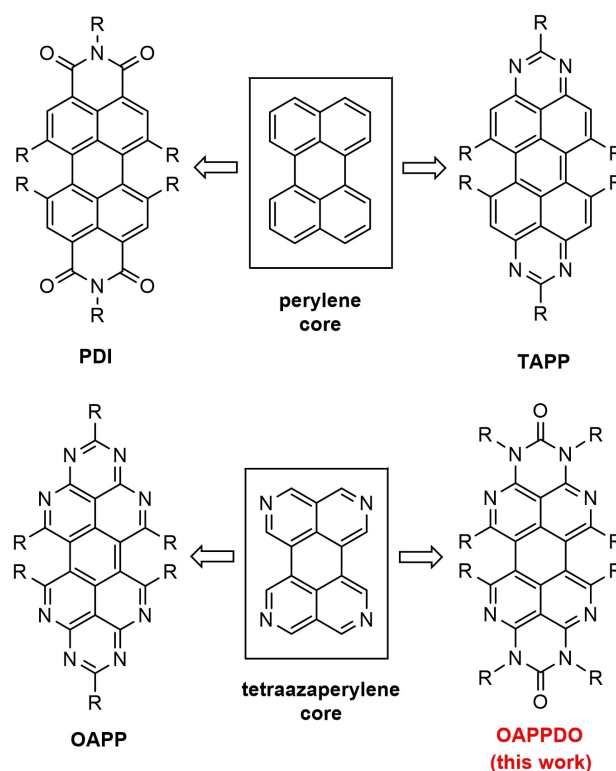
**Abstract:** Octaazaperopyrenedioxides (OAPPDOs) are a new class of fluorescent polycyclic aromatic hydrocarbons based on a tetraazaperylene core that is formally condensed with N-substituted urea units in the two opposite *peri* positions. Here, we report the synthesis of series of substituted OAPPDO derivatives with different N-substitution patterns (H, alkyl, benzyl) in the *peri* positions, including bay-chlorinated OAPPDOs. Starting from the latter, a series of bay-arylated OAPPDOs was synthesized by Suzuki cross coupling, which resulted in the formation of helically chiral OAPPDO derivatives. The electrochemical and photophysical properties were

investigated by UV/Vis and fluorescence spectroscopy as well as cyclic voltammetry. The *P* and *M* enantiomers of a phenylated OAPPDO were separated by semipreparative HPLC and further analyzed by CD spectroscopy. The frontier orbital energies, the mechanism of the isomerization, the electronic excitation and the CD spectrum (TD-DFT) were computed and compared to the experimental data. The reversible  $1e^-$  oxidation of the OAPPDOs generates the corresponding radical cations, one of which was characterized by EPR spectroscopy. The reversible oxidation process was also systematically investigated by spectro-electrochemistry.

## Introduction

The perylene core is the central structural motif of a highly developed class of functional dyes and pigments. In particular, perylene tetracarboxydiimides (PDIs) have been extensively studied for more than a century.<sup>[1–5]</sup> The high impact of the PDIs as molecular organic materials is rooted in their excellent functional properties relevant to opto-electronic applications, the possibility to tune these properties on the molecular level as well as their thermal and photochemical stability.<sup>[2–3,5–20]</sup>

The electron-withdrawing dicarboximide substituents in the *peri* positions of the perylene core in PDIs renders these dyes electron acceptors which have made them attractive materials for application as organic n-channel semiconductors in OFETs.<sup>[21–25]</sup> Analogous behavior has been established for the closely related class of dyes in which the terminal *peri* dicarboximides have been replaced by the condensation of pyrimidine rings at opposite ends of the perylene core giving rise to tetraazaperopyrenes (TAPPs; Scheme 1, top).<sup>[26–36]</sup> The latter class of compounds may also be viewed as derived from the peropyrene reference system by fourfold [CH→N] replacement,<sup>[26–36]</sup> rendering the polycyclic aromatics electron



**Scheme 1.** Functional dyes based on a perylene core, PDIs and TAPPs (top) and a central tetraazaperylene unit, OAPPs and OAPPDOs (bottom). Bay functionalization leads to twisted chiral aromatic cores.

acceptors. This strategy of isosteric [CH→N] replacement has allowed the tuning of the molecular redox properties without

[a] T. Wesp, T. Bruckhoff, Prof. H. Wadepohl, Prof. L. H. Gade  
Anorganisch-Chemisches-Institut, Universität Heidelberg  
Im Neuenheimer Feld 270, 69120 Heidelberg (Germany)  
E-mail: lutz.gade@uni-heidelberg.de

Supporting information for this article is available on the WWW under <https://doi.org/10.1002/chem.202201706>

© 2022 The Authors. Chemistry - A European Journal published by Wiley-VCH GmbH. This is an open access article under the terms of the Creative Commons Attribution Non-Commercial License, which permits use, distribution and reproduction in any medium, provided the original work is properly cited and is not used for commercial purposes.

extensive modification of the peripheral substituents but rather within the poly(N-heterocyclic) aromatic core itself.<sup>[37–42]</sup>

Recently, we have begun to extend the construction principle outlined above to dyes based on a *tetraazaperylene* core (Scheme 1, bottom), thus reducing the frontier orbital energies by [CH→N] replacement within the central aromatic polycycle.<sup>[43]</sup> Further modification following the synthetic routes to the previously studied TAPPs gave access to the nitrogen rich, strongly electron-accepting octaazaperopyrenes (OAPPs) for which a first assessment of their properties has been reported.<sup>[43]</sup>

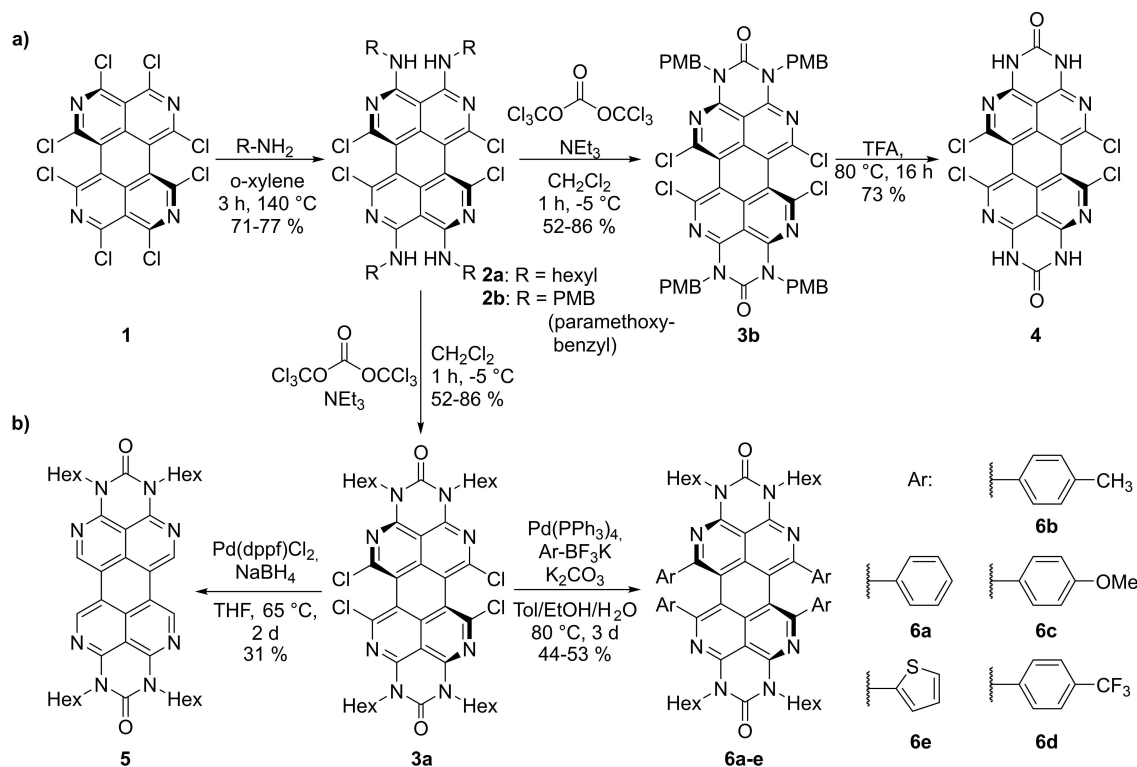
Based on the tetraazaperylene core we have now added N-substituted urea units in the *peri* positions, thus generating a periphery which is complementary to the dicarboximido termini in the PDIs. Similar to the latter, the combination of NH– and carbonyl functions allows the formation of intermolecular hydrogen bonds which ultimately is expected to lead to stable, tightly packed materials.<sup>[39,44–47]</sup> This new class of dyes may be viewed as formally derived from the recently reported octaazaperopyrenes by oxidation of the two axial CH units and is therefore referred to as octaazaperopyrenedioxides (OAPPDO).<sup>[43]</sup> Specifically, we report the synthesis of a bay-halogenated OAPPDO derivative which has offered the opportunity for further functionalization and, in particular, freezing in the twisted conformation of the polycyclic aromatic core. This has led to the isolation of helically chiral OAPPDO dyes.

## Results and Discussion

### Synthesis of octaazaperopyrenedioxides

The octachlorotetraazaperylene **1**, previously employed in the synthesis of octaazaperopyrenes (OAPPs) is an excellent starting compound for the OAPPDO target compounds, given that different nucleophiles were found to attack exclusively at the *peri* position.<sup>[48]</sup> Compound **2b** was obtained in good yields by reaction of **1** with *para*-methoxybenzylamine. In contrast to the perchlorinated perylene, compound **2b** is highly soluble in common organic solvents. In the next step the amine **2b** was reacted with triphosgene to give the OAPPDO derivative **3b** (Scheme 2). In all compounds the aromatic core is twisted as a result of the steric pressure of the chlorine substituents in the bay position. The resulting racemate of two enantiomers (*P+M*) could not be separated due to their thermal interconversion at subambient temperature.<sup>[49]</sup> Finally, the N-substituent-free compound **4** was synthesized by acid-catalyzed deprotection of the benzyl group of **3b** with trifluoroacetic acid and found to be poorly soluble in common organic solvents which complicated further functionalization in the bay position.

The lability of the *para*-methoxybenzyl-*N* substituents under the reaction conditions for further bay functionalization led us to repeat the reaction sequence starting from **1** by the reaction with hexylamine to give compound **2a**, which was subsequently converted with triphosgene to the corresponding OAPPDO **3a**.<sup>[50]</sup> For this highly soluble compound **3a**, it was



**Scheme 2.** a) Synthetic route to the parent compound OAPPDO **4** as well as b) the cross coupled derivatives **6** and the dehalogenated, planarized compound **5**.

possible to substitute the bay position by palladium-catalyzed Suzuki coupling. To this end, aryl fluoroborates were used as transmetalation reagents in the presence of potassium carbonate and a catalytic amount of  $\text{Pd}(\text{PPh}_3)_4$  (Scheme 2) yielding the coupled derivatives **6a–e**.<sup>[51–53]</sup> On the other hand, the bay-unsubstituted compound OAPPDO **5** was synthesized by palladium-catalyzed dehalogenation, which resulted in planarization of the aromatic core.<sup>[54]</sup> For the latter transformation, sodium borohydride was found to be suitable as a reducing reagent with  $\text{Pd}(\text{dppf})\text{Cl}_2$  as precatalyst.

The crude mass spectra of compound **6a** indicated the formation of a Suzuki coupled derivative with subsequent intramolecular C–H activation as by-products.<sup>[55]</sup> The reaction parameters were therefore modified to specifically target an azadibenzocoronene starting from **3a** (Scheme 3). Instead of a significant excess of the borane reagent, as used in the synthesis of **6a–e** only two equivalents were used. From this reaction the partially condensed and partially dehalogenated compound **8a** was isolated in low yield. To avoid the protodehalogenation, that prevented a second C–H activation and ring closure, Stille conditions were applied, thus circumventing the use of a protic solvent. However, whereas protodehalogenation was successfully avoided, only one C–H activation step occurred to give the asymmetric compound **7a** (Scheme 3). To which degree this approach may be modified to obtain the targeted coronene derivative therefore remains to be established in future work.

### Crystal structures of the OAPPDO derivatives **6a–d**

Single crystals of the bay-arylated OAPPDOs **6a–d** were grown by slow evaporation of a concentrated *n*-hexane/ $\text{CH}_2\text{Cl}_2$  solution (Figure 1), to establish the details of the molecular structures as well as their packing in the solid state. The racemic mixtures of the chiral OAPPDOs **6a–d** were used for the crystallization in all cases.

All molecular structures were found to be characterized by a strong distortion of the azaperylene core, with the relevant torsion angle  $\Phi$  being between  $26.8^\circ$  (**6d**) and  $30.9^\circ$  (**6c**; Table 1). The twist results from the steric pressure of the two

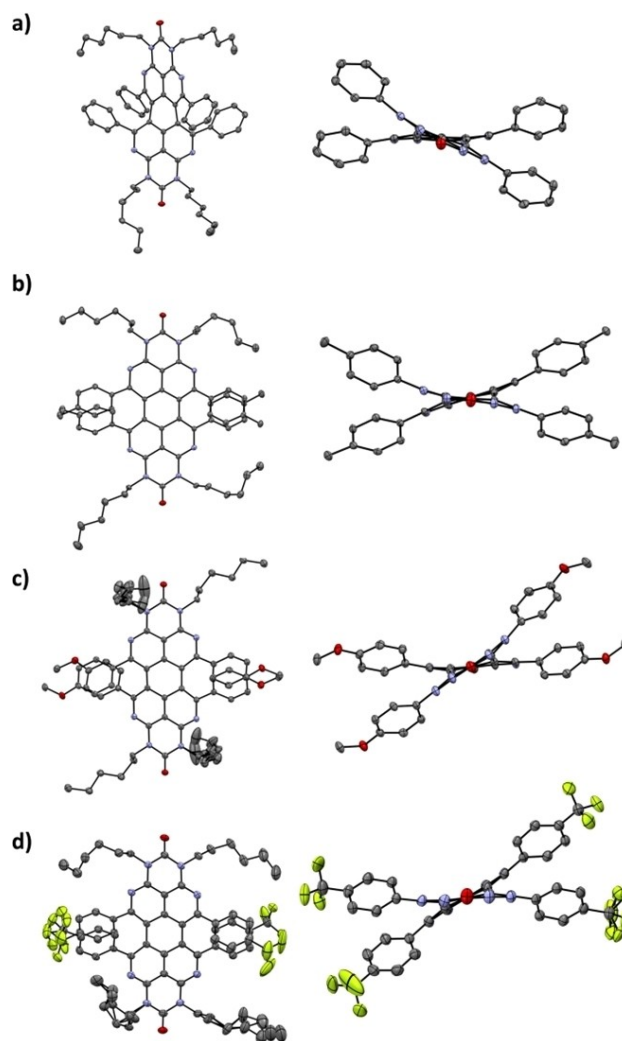
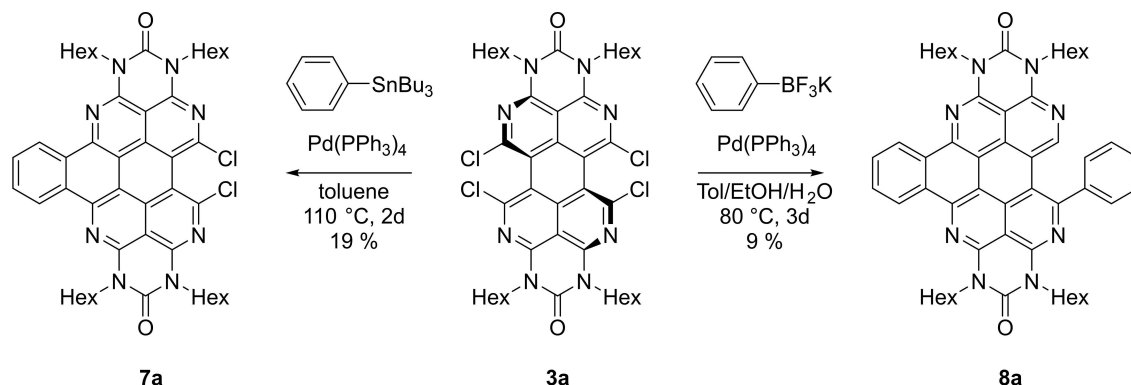


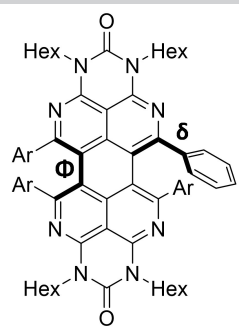
**Figure 1.** Solid-state structures of bay-arylated OAPPDOs a) **6a**, b) **6b**, c) **6c**, and d) **6d**. The molecular structure is displayed on the left; the twist of the azaperylene core is shown on the right (the hexyl groups are omitted for clarity).

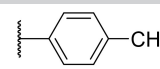
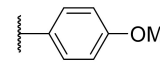
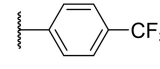
aryl groups on each side, but happens to be slightly smaller than for the corresponding bay-chlorinated tetraazaperylene **1**



**Scheme 3.** Synthetic investigations to obtain an octaazacoronene derivative.

**Table 1.** Structural parameters of solid-state structures of **6a–d**.



Ar:  **6b**  
 **6a**  **6c**  
 **6e**  **6d**

|           | Space group                       | Torsion angle <sup>[a]</sup> |              | Torsion angle <sup>[b]</sup> |                     |
|-----------|-----------------------------------|------------------------------|--------------|------------------------------|---------------------|
|           |                                   | $\Phi_1$ [°]                 | $\Phi_2$ [°] | $\delta_{\min}$ [°]          | $\delta_{\max}$ [°] |
| <b>6a</b> | <i>P</i> $\bar{1}$                | 26.8(7)                      | 28.6(1)      | 37.0(4)                      | 43.4(8)             |
| <b>6b</b> | <i>P2</i> <sub>1</sub> / <i>c</i> | 27.9(2)                      | 28.7(2)      | 39.1(2)                      | 43.1(2)             |
| <b>6c</b> | <i>I2/a</i>                       | 30.9(2)                      | 30.9(2)      | 35.4(2)                      | 41.7(2)             |
| <b>6d</b> | <i>P</i> $\bar{1}$                | 27.4(4)                      | 28.8(4)      | 42.0(4)                      | 43.7(3)             |

[a] Torsion angles  $\Phi$  were measured between the tetraazaphthalenylone units of one molecule. [b] Torsion angles  $\delta$  were measured between a tetraazaphthalenylone and the corresponding aryl subunit.

(36.1°)<sup>[56]</sup> or previously synthesized bay-chlorinated TAPP (29.4–32.4 Å)<sup>[34]</sup>/OAPP (33.7°) derivatives.<sup>[56]</sup> This can be explained by an attractive interaction of the aryl units for which a distance between the centroids of the aryl rings of 3.5–3.6 Å was found, suggesting weak  $\pi$ – $\pi$  interactions between the aryl substituents despite the fact that these are not arranged parallel to each other. Furthermore, the aryl substituents are tilted from the naphthyridine planes by the dihedral angle  $\delta$  of 35–43° (Table 1) which largely suppresses conjugation of the aryl groups with the central tetraazaperylene core.

In contrast to the structurally similar bay-chlorinated TAPP derivatives,<sup>[34]</sup> the C–C bond length between the two naphthyridine units in **6a–d** was found to be elongated (1.42 Å for the TAPP<sup>[34]</sup> vs. 1.47 Å for the OAPPDOs). This untypically long C–C bond indicates only a partial delocalization of the  $\pi$ -system over the complete azaperylene core. Despite the twist of the azaperylene core, the individual naphthyridine units do not show additional strain and the other aromatic C–C bonds possess typical bond lengths. The distortion and rotation angles of the ( $\Phi$  and  $\delta$ ) structures are summarized in Table 1.

The solid-state packing patterns of the OAPPDOs **6a–d** and the corresponding inter-layer distances are displayed in Figure 2. For all derivatives, no  $\pi$ – $\pi$  stacking of the azaperylene core was observed due to the steric hindrance of the protruding aryl units. This is in contrast to previously described TAPP derivatives.<sup>[56,34]</sup> In general, the steric hindrance of the hexyl and aryl groups leads to large interlayer distances between 8–10 Å.

Compound **6a** exhibits a brick layer stacking (inter-layer distance of 4.2 Å) of the azaperylene units. Notably, the packing motif varies for the different *para*-substituted derivatives in spite of their similar molecular structures. For **6b** the layers (8.2 Å) are parallel-displaced and within a layer the OAPPDOs of neighboring molecules are alternately shifted with respect to each other. In contrast to **6a,b**, two of the hexyl groups of **6c** are orientated perpendicularly to the azaperylene core. Con-

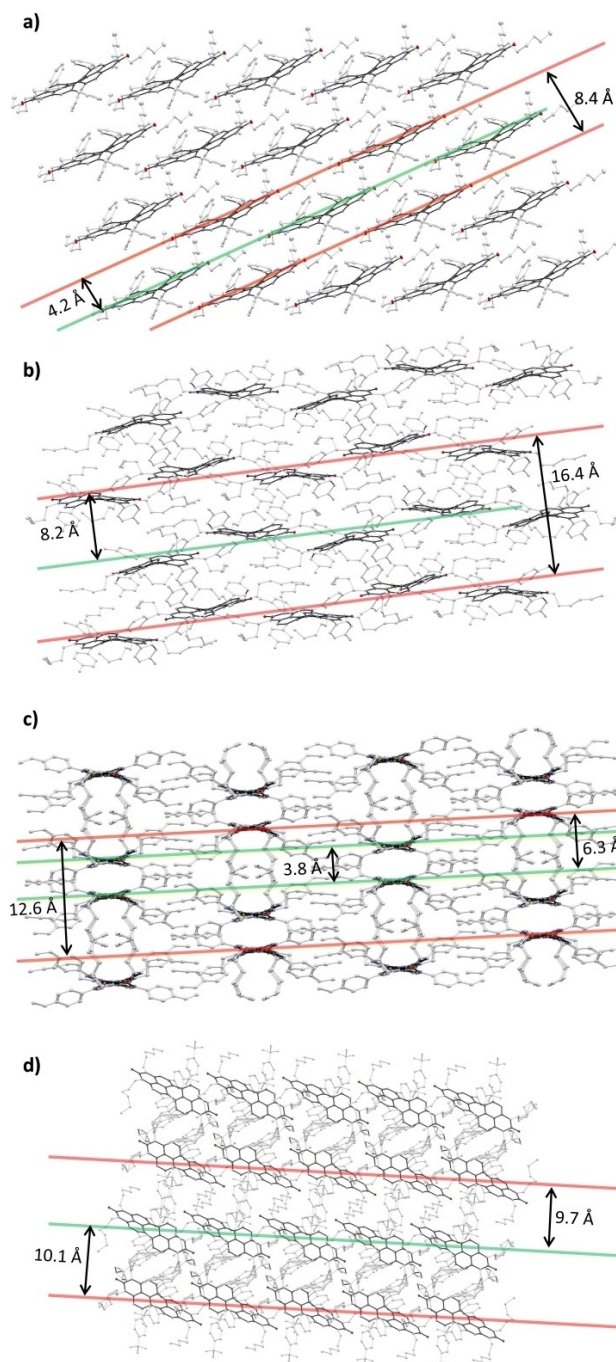


**Figure 2.** Molecular packing of a) **6a**, b) **6b**, c) **6c**, and d) **6d**.

sequently, the OAPPDOs of neighboring layers are arranged back to back and shifted in parallel displacement. For **6d**, the OAPPDO units within a layer are arranged parallel and in contrast to the other derivatives, they are not orientated in a zigzag pattern. The adjacent layer is shifted parallel with the OAPPDO core being rotated but localized off-center relative to the neighboring layers (Figure 2d).

### Conformation analysis

The steric repulsion of the aryl substituents in the bay position leads to the twist of the perylene core and consequently, to the formation of helically chiral structures.<sup>[49,53, 57–58,59]</sup> There are thus two atropisomers (*P* and *M*) of compounds **6a–e**. Due to this helical chirality, the proton signals of the bay aryl units in the <sup>1</sup>H NMR spectra are not equivalent and appear separated at low temperature (Figure 3, –30 °C). At temperatures below –30 °C, the exchange of the *ortho* protons was frozen due to the decelerated rotation of the aryl unit, resulting in two different signals for the *ortho* protons (7.43 and 6.90 ppm). Upon heating to 20 °C, the *ortho* proton resonances coalesced, while the *meta* protons exhibit sharp signals. The latter can be explained by their larger distance from the chiral core, thus reducing the effect of the resulting diastereotopicity. The coalescence temperature is at 293 K corresponding to a rotational barrier  $\Delta G^\ddagger$  of 56.7 kJ mol<sup>–1</sup> (13.5 kcal), which is in accordance with

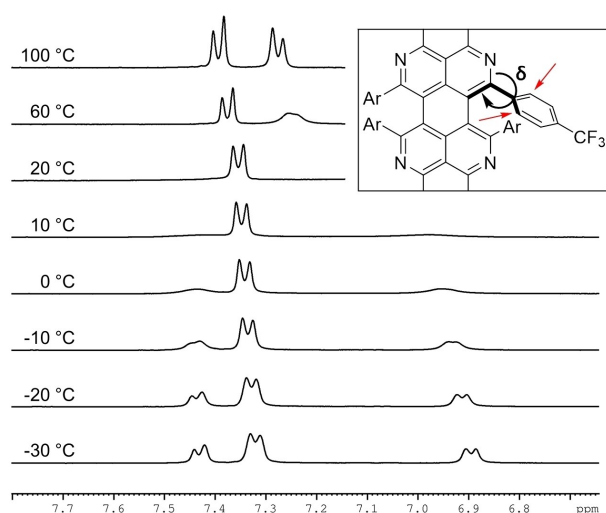


**Figure 3.** Temperature-dependent <sup>1</sup>H NMR spectrum of the 4-trifluorophenyl resonances of compound **6d** in [D<sub>2</sub>]TCE.

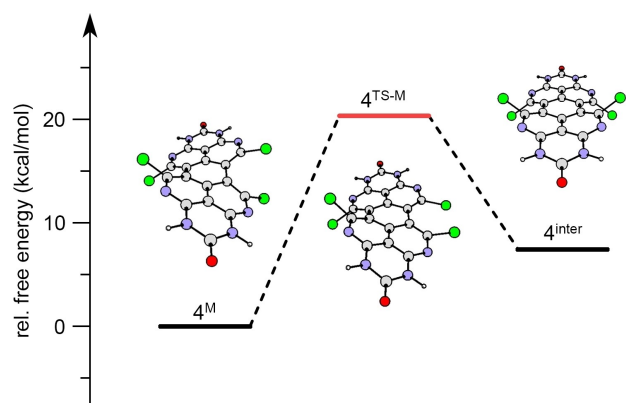


**Figure 4.** DFT-modeled energy profile (B3LYP-GD3(BJ)/Def2-TZVP) for the isomerization of **4<sup>M</sup>**→**4<sup>P</sup>**. Only the part of the mechanism leading to intermediate **4<sup>inter</sup>** is shown, due to the symmetrical character of the isomerization.

previous observations made for similar PDI derivatives.<sup>[53]</sup> Further heating resulted in the formation of a sharp doublet for the *ortho* protons which corresponds to the expected dynamic high temperature limit.

The helical isomerism of the structures **3a**, **4**, **5** and **6a–e** was also studied by DFT calculations employing B3LYP-GD3(BJ)/Def2-SVP<sup>[60–66]</sup> or B3LYP-GD3(BJ)/Def2-TZVP<sup>[60–66]</sup> (for details see the Supporting Information). Figure 4 displays an example of the isomerization mechanism for compound **4**. All compounds isomerize according to an identical and symmetric pathway. Starting from one of the atropisomers (*M* or *P*), the bay substituents first pass on one side (TS), leading to an achiral intermediate (*inter*). For a potential concerted exchange of the bay substituents, which would correspond to an inversion with only one transition state, no reaction trajectory was found in the model studies. This is in line with previous findings for the inversion mechanism of bay-chlorinated perylenes.<sup>[34]</sup> Starting from the intermediate structure, the other stereoisomer is obtained via a mirrored transition state with the same energy barrier.

Due to the high number of degrees of freedom and many energetically close conformations, the hexyl substituents were replaced by methyl groups in the DFT models. It was assumed that for the bay-arylated OAPPDOs, the influence of the hexyl chain on the energy level of the transition states should be higher than for the nonarylated. To estimate the influence of the hexyl groups, seven distinguishable conformers with linear hexyl chains were considered for the ground state structures of **6a**, representing ground state energies differing by up to 2.2 kcal mol<sup>–1</sup> (B3LYP-GD3(BJ)/Def2-TZVP). Comparison of the transition states of the methyl- and hexyl-substituted structures revealed energy differences of up to 2.9 kcal mol<sup>–1</sup> (B3LYP-GD3(BJ)/Def2-TZVP).

To reduce the computational cost, the mechanisms of all derivatives were computed using the basis set Def2-SVP. Here, energy barriers are obtained that deviate by <0.8 kcal mol<sup>–1</sup> from those calculated with Def2-TZVP. The low transition barrier for the bay-chlorinated compound **3a** ( $\Delta G^\ddagger = 19.8$  kcal mol<sup>–1</sup>) is in accordance with the experimental finding of the inversion at room temperature. In contrast, the calculated energy barriers of the compounds with the bulky bay aryl substituents range from 26.2 to 28.7 kcal mol<sup>–1</sup>. The calculated energy barrier for compound **6d** is slightly larger than the experimentally energy barrier of 25.9 kcal mol<sup>–1</sup> determined by variable temperature circular dichroism (see the Supporting Information).

For a frozen twist in the tetraazaperylene core, the energy barrier of rotation of the *para*-trifluoromethylphenyl was computed to be 15.7 kcal mol<sup>–1</sup> at the B3LYP-GD3(BJ)/Def2-SVP level of theory, which is 2.2 kcal mol<sup>–1</sup> higher than the experimentally determined barrier.

### UV/Vis absorption and emission spectra

The different OAPPDOs are dyes with absorption bands in the visible spectral region which exhibit molar absorption coefficients between 14 000 and 32 000 M<sup>–1</sup>cm<sup>–1</sup> in CH<sub>2</sub>Cl<sub>2</sub>. The bay-

chlorinated OAPPDO **3a** possesses a broad absorption band with a maximum of 494 nm (Figure 5a) and a vibrational progression towards shorter wavelengths. Both compounds are highly fluorescent with the emission band being Stokes shifted by  $900\text{ cm}^{-1}$  (Figure 5a).

The comparison of the alkylated (**3a**), benzylated (**3b**), and N-protonated OAPPDO (**4**; see the Supporting Information) indicates that the absorption maxima are nearly independent of the “urea” nitrogen substituents. Compared to **3a** the dehalogenation of the bay position and the resulting planarization (**5**) leads to a small blue shift of 7 nm of the absorption and 24 nm of the corresponding emission maxima. Although there is only a small difference in the absorption and emission spectra of compound **3** and **5**, the fluorescence quantum yield is decreased by 40% for the latter.

The arylation of the bay position leads to an additional intense, broadened band at 425 nm in the absorption spectra

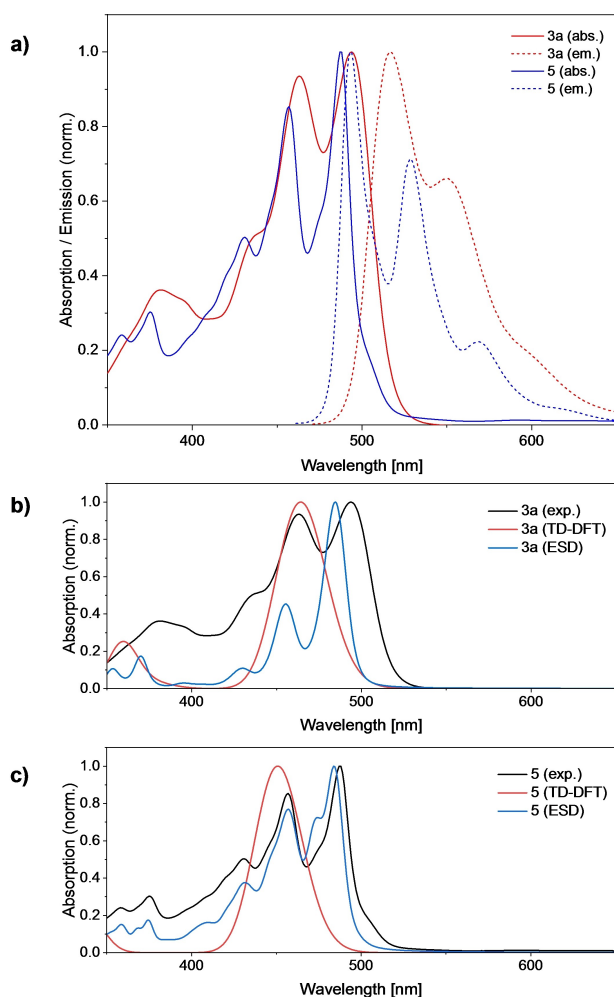


**Figure 5.** a) Experimental absorption and emission spectra of compounds **3a** and **5**. Predicted absorption spectra employing purely TD-DFT (B3LYP-GD3(BJ)/Def2-TZVPP) and including excited-state dynamics (ESD; B3LYP-GD3(BJ)/Def2-SVP), that is, vibronic coupling, are depicted together with their respective experimental spectrum for compounds (b) **3a** and (c) **5**. ESD spectra were corrected by the energy difference of the first singlet excited state in TD-DFT calculations on double- or triple- $\zeta$  level of theory.

(Figure 6a). These absorption maxima are almost identical for all phenyl substituted derivatives **6a–d**, whereas the thiophene substitution in derivative **6e** induces a red shift of 25 nm in the absorption spectrum and even a larger red shift in the emission spectrum (50 nm). All arylated OAPPDOs **6a–e** exhibit large Stokes shifts of more than  $2700\text{ cm}^{-1}$  for the emission bands which can be explained by the strong twist of the molecule and the resulting additional internal degrees of freedom.

The semiplanarization of the perylene core leads to a blue shift of the absorption maximum of 36 nm in **7** and 38 nm in **8** in comparison to the parent compound **3a**. Compared to compound **7**, the additional phenyl unit in **8** shifted the emission maximum to significantly higher wavelengths (see Table 2 the Supporting Information).

The experimental UV/Vis spectra depicted in Figure 5a and 6a were modeled by TD-DFT (B3LYP-GD3(BJ)/Def2-TZVPP)<sup>[60–66]</sup> to investigate the character of the electronic excitations in more detail (Figures 5b, c and 6b). According to the TD-DFT calculations, the absorption maximum of lowest energy corresponds to the first singlet transition ( $S_0 \rightarrow S_1$ ) for all compounds. The energetically significant higher excitations  $S_0 \rightarrow S_2$  (and  $S_0 \rightarrow S_3$ , only for **3a** and **5**) are weakly or non-dipole allowed, while the next higher, dipole allowed singlet excitations correspond either to the absorption bands at  $\lambda_{\text{max}}$  in **6a–e** (Figure 6b) or those at 375–380 nm in **3a** or **5** (Figure 5b, c).

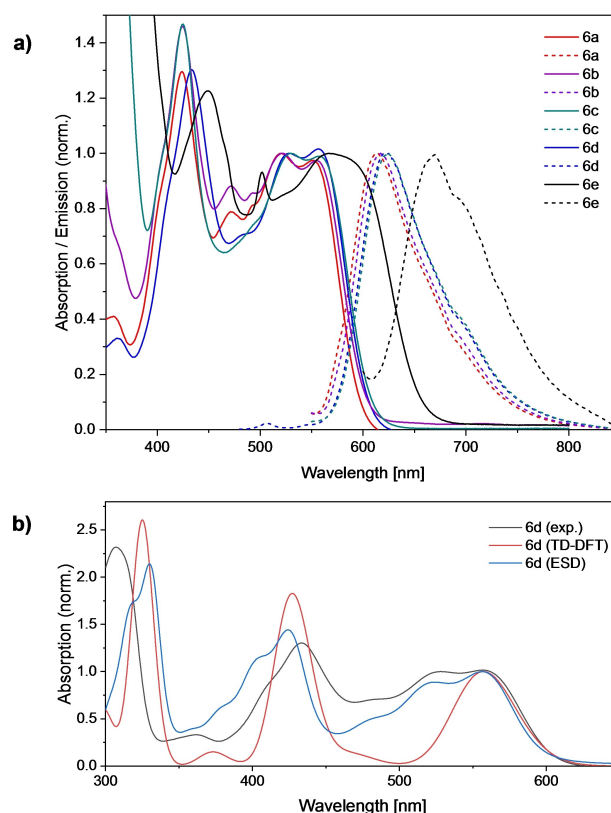


**Figure 6.** a) Absorption (full lines) and emission (dotted lines) spectra of compounds **6a–e**. b) Predicted absorption spectra employing purely TD-DFT (B3LYP-GD3(BJ)/Def2-TZVPP) and including ESD (B3LYP-GD3(BJ)/Def2-SVP), that is, vibronic coupling, are depicted together with their corresponding experimental spectrum for compound **6d**.

**Table 2.** Photophysical properties of 3–8 in CH<sub>2</sub>Cl<sub>2</sub> at room temperature.

|           | $\lambda_{\text{abs,max}}$ [nm]<br>(log $\epsilon$ ) <sup>[a]</sup> | $\lambda_{\text{em,max}}$ [nm]<br>( $\Phi_{\text{em}}$ ) <sup>[b]</sup> | 0–0 Transition<br>[nm] | Stokes shift<br>[cm <sup>-1</sup> ] |
|-----------|---|---|------------------------|-------------------------------------|
| <b>3a</b> | 494 (4.51)  | 517 (67 %)  | 505                    | 901                                 |
| <b>3b</b> | 495 (4.38)  | 518 (77 %)  | 507                    | 897                                 |
| <b>4</b>  | 489 (4.29)  | 512 (60 %)  | 501                    | 918                                 |
| <b>5</b>  | 487 (4.40)  | 493 (30 %)  | 490                    | 250                                 |
| <b>6a</b> | 424 (4.17)  | 614 (34 %)  | 580                    | 2907                                |
| <b>6b</b> | 425 (4.33)  | 617 (37 %)  | 583                    | 2986                                |
| <b>6c</b> | 425 (4.25)  | 624 (33 %)  | 588                    | 2842                                |
| <b>6d</b> | 433 (4.32)  | 622 (33 %)  | 588                    | 2862                                |
| <b>6e</b> | 449 (4.14)  | 671 (5 %)   | 630                    | 2734                                |
| <b>7</b>  | 458 (4.49)  | 494 (5 %)   | 472                    | 1591                                |
| <b>8</b>  | 456 (4.45)  | 534 (28 %)  | 489                    | 3203                                |

[a] Spectra were recorded in CH<sub>2</sub>Cl<sub>2</sub> ( $c \approx 10^{-5}$  M). [b] Fluorescence quantum yields were measured with an Ulbricht sphere (extinction  $E < 0.1$ ).

The additional spectral features can be explained by dynamic effects such as vibronic coupling (Herzberg–Teller effect),<sup>[67–70]</sup> as it is known for other polycyclic hydrocarbons such as pyrene.<sup>[71–73]</sup> For the qualitative insight, the vibronic coupling was computed between the ground state ( $S_0$ ) and the excited states  $S_1$  up to  $S_5$  (for **3a** or **5**) or  $S_3$  (for **6d**) using the vertical gradient model as implemented in the ORCA\_ESD (excited state dynamics) module<sup>[74]</sup> at B3LYP-GD3(BJ)/Def2-SVP level of theory (for details see Section 3.2.2 in the Supporting Information).

### Chiroptical properties

The tetraphenylated OAPPDOs exist as their *P* and *M* atropisomers with an axial chirality. Both enantiomers are configurationally stable at room temperature which can be explained by the steric demand of the aryl groups.<sup>[49]</sup> Consequently, enantiomers were expected to be separable using enantiomeric separation techniques. As an example, compound **6d** was separated by semi preparative HPLC using a column packed with amylose tris( $\alpha$ -methylbenzylcarbamate) coated on silica gel (AS–H). The circular dichroism spectra for both enantiomers are displayed in Figure 7. As expected the enantiomers displayed a mirror image relation with an intense band at 310 nm and a broad band between 450 and 600 nm. Based on the structural and electronic similarity to the PDIs, the band between 450 and 600 nm can be assigned to the  $S_0 \rightarrow S_{1,2}$ .<sup>[53,55,57]</sup> The sign of this band indicates the absolute configuration of the  $D_2$  symmetrical enantiomers.<sup>[55,75–77]</sup> *P* chirality was assigned for a positive band whereas a negative sign was attributed to the *M* enantiomer.<sup>[53,55,57,58,78]</sup> The assignments of the enantiomers were confirmed by a comparison of the computed TD-DFT CD spectrum at B3LYP-GD3(BJ)/Def2-TZVPP level of theory with CPCM<sup>[79–80]</sup> as solvation model for hexane (Figure 7). The *P* enantiomer exhibits a positive Cotton effect for the lowest energy transition and the *M* enantiomer a negative one.

The characteristics of the electronic transitions in **6d** were further investigated by analyzing the interfragment charge transfer of the first eight excited states in the TD-DFT

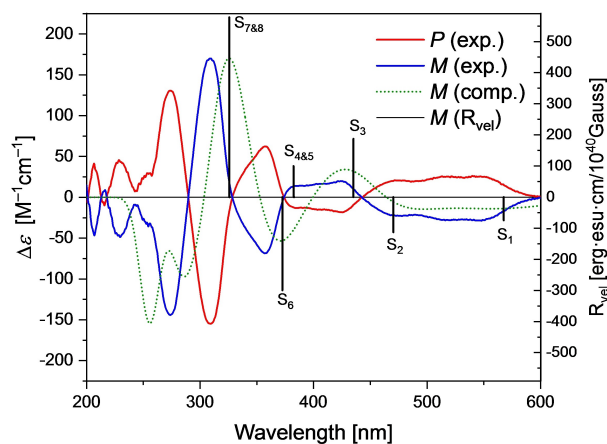


**Figure 7.** Experimental circular dichroism (CD;  $c_0 = 3.3 \times 10^{-5}$  M) spectrum and TD-DFT-predicted spectrum (comp., B3LYP-GD3(BJ)/Def2-TZVPP/CPCM<sub>hexane</sub>) of **6d** in *n*-hexane. The maximum at 326 nm of the computed spectrum was normalized to the corresponding maximum of the experimental spectrum. Rotatory strength ( $R_{\text{vel}}$ ) was reported for the first eight singlet excitations.

calculation (for details see the Supporting Information). According to the calculated CD spectrum, the first band corresponds to the  $S_0 \rightarrow S_1$  and  $S_0 \rightarrow S_2$  excitation, while the second band arises from the transition  $S_0 \rightarrow S_3$ . All three excitations correspond to centrosymmetric charge transfer mainly localized in the peropyrene core but with increasing donation into the aryl-substituents. The singlet transitions  $S_0 \rightarrow S_4$  and  $S_0 \rightarrow S_7$  have nearly no rotatory strength and thus do not contribute to the CD spectrum. The third band can be assigned to the excitations of  $S_0 \rightarrow S_5$  and  $S_6$ , which is characterized by local excitations in the peropyrene core with low charge transfer between the core and aryl fragments. The fourth band is almost exclusively related to the  $S_0 \rightarrow S_8$  transition with significant charge transfer from the aryl substituents into the peropyrene core. However, the excitation energies of the  $S_0 \rightarrow S_6$  and  $S_8$  transitions seem to be underestimated on the chosen level of theory and thus  $S_5$  might contribute to the second band.

### Redox properties

The redox properties of the OAPPDOs were investigated by cyclic voltammetry in CH<sub>2</sub>Cl<sub>2</sub>, using tetrabutylammonium hexafluorophosphate as an electrolyte and a scanning calomel electrode (SCE) as a reference electrode. The key data are summarized in Table 3 and referenced on Fc/Fc<sup>+</sup>.

In contrast to the TAPPs and the structurally related OAPPs, which are strong electron acceptors, the parent compound **3a** revealed two separate one electron oxidation steps in the cyclic voltammogram but no reduction waves at negative potential (Figure 8; left). Both oxidation steps (0.65 and 0.84 V) are reversible. The oxidation steps can be assigned to the formation of the radical cation and dication which results from the oxidation of the aromatic core. The oxidation of the OAPPDOs is favored compared to the TAPPs and compound **1** because

|           | EA (DFT) <sup>[a]</sup><br>[eV] | $E_{\text{HOMO}}$ (DFT) <sup>[b]</sup><br>[eV] | $E_{\text{LUMO}}$ (DFT) <sup>[b]</sup><br>[eV] | $E_{\text{opt}}$ (TD-DFT) <sup>[c]</sup><br>[eV] | $E_{\text{OX1}}$ <sup>[d]</sup><br>[V] | $E_{\text{OX2}}$ <sup>[d]</sup><br>[V] | $E_{\text{HOMO}}$ (CV) <sup>[e]</sup><br>[eV] | $E_{\text{HOMO-LUMO}}$ (UV/Vis) <sup>[f]</sup><br>[eV] |
|-----------|---------------------------------|--|--|--|--|--|---|--|
| <b>3a</b> | 2.73                            | −5.64  | −2.60  | 2.67   | 0.654                                  | 0.838                                  | −5.80   | 2.38   |
| <b>5</b>  | 2.39                            | −5.32  | −2.28  | 2.75   | 0.391                                  | 0.628                                  | −5.54   | 2.46   |
| <b>6a</b> | 2.59                            | −5.13  | −2.44  | 2.25   | 0.197                                  | 0.435                                  | −5.35   | 2.07   |
| <b>6b</b> | 2.52                            | −5.05  | −2.37  | 2.24   | 0.155                                  | 0.390                                  | −5.31   | 2.06   |
| <b>6c</b> | 2.45                            | −4.96  | −2.30  | 2.20   | 0.115                                  | 0.336                                  | −5.27   | 2.04   |
| <b>6d</b> | 2.90                            | −5.38  | −2.73  | 2.23   | — <sup>[g]</sup>                       | — <sup>[g]</sup>                       | — <sup>[g]</sup>                              | 2.05   |
| <b>6e</b> | 2.77                            | −5.07  | −2.59  | 2.02   | 0.191                                  | 0.393                                  | −5.34   | 1.89   |

[a] Electron affinities were calculated using the  $\Delta\text{SCF/DFT}$  approach<sup>[83]</sup> as  $EA = E_{\text{neut}} - E_{\text{red}}$  employing B3LYP-GD3(BJ)/Def2-TZVP/CPCM<sub>DCM</sub> ( $E_{\text{neut/red}}$  refer to the total SCF energies of the neutral or reduced compound). [b] Properties were calculated as the SCF-orbital energies of the neutral compound at B3LYP-GD3(BJ)/Def2-TZVP/CPCM<sub>DCM</sub> level of theory. [c] The optical band gap ( $E_{\text{opt}}$ ) was obtained as the  $S_0 \rightarrow S_1$  singlet excitation from TD-DFT (B3LYP-GD3(BJ)/Def2-TZVP). [d] Half-wave potentials were measured by cyclic voltammetry in  $\text{CH}_2\text{Cl}_2$  using tetrabutylammonium hexafluorophosphate as electrolyte and the redox potential of ferrocene as reference. [e] HOMO energy was calculated from the reversible first oxidation potential according to a literature known procedure ( $E_{\text{HOMO}} = -[E_{\text{OX1}} + 5.15 \text{ eV}]$ ).<sup>[53]</sup> [f] Calculated from  $\lambda_{\text{onset}}$  of the UV/Vis spectrum. [g] No reversible oxidation potential was observed.

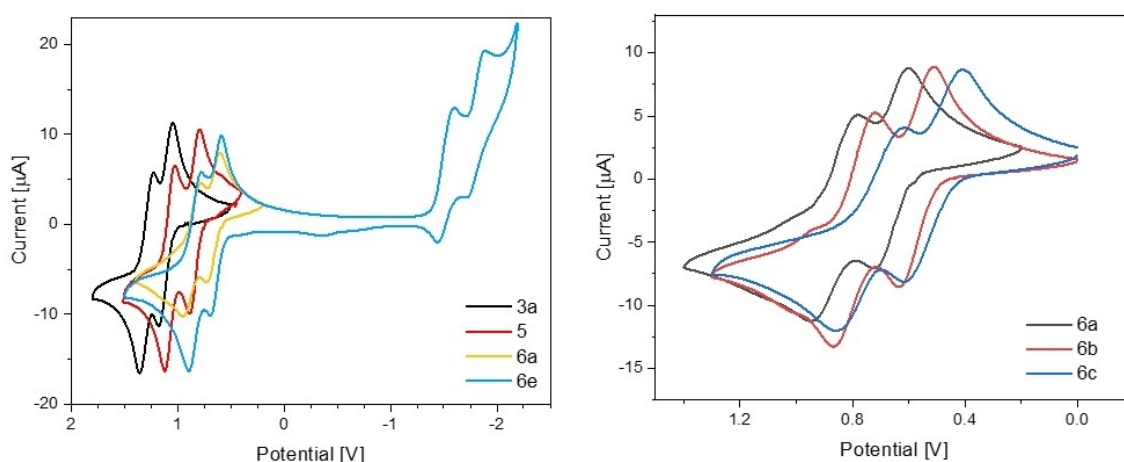


**Figure 8.** Left: Cyclic voltammograms of **3a**, **5**, **6a**, **6e** measured in  $\text{CH}_2\text{Cl}_2$ , supp. Electrolyte:  $\text{Bu}_4\text{NPF}_6$ , reference SCE, sweep rate  $50 \text{ mV s}^{-1}$ . Right: Comparison of the oxidation potential depending on the *para* substituent of the aryl unit of **6a–c**.

the central (tetraaza)perylene core represents a formally reduced form. Additionally the amidation of the *peri* position has introduced substituents exerting a +M effect. The bay-chlorinated OAPPDO **3** was found to exhibit the highest oxidation potential because of the negative inductive effect of the chlorine substituents, whereas its dehalogenation to **5** shifted the oxidation waves to lower potentials, thus indicating a stabilization of the radical cation and twofold oxidized species.

Arylating the bay position shifted both oxidation waves to even lower potentials. The two oxidation steps of the arylated derivatives **6a–c,e** were observed at 0.12–0.20 V and 0.34–0.44 V, respectively (Figure 8, right). In contrast to the electron-donating substituents of **6a–c** only one irreversible oxidation wave was observed for *para*- $\text{CF}_3$ -substituted compound **6d** (see the Supporting Information). In contrast to the phenylated derivatives, two quasireversible reduction waves ( $E_{\text{red}}^1 = -1.52 \text{ V}$ ,  $E_{\text{red}}^2 = -1.81 \text{ V}$ ) were additionally observed for the thiophene coupled compound **6e**. Based on a well established method in the literature, the energy of the HOMO was estimated from the measured potential of the first oxidation step ( $E_{\text{OX1}}$ ) referenced

to  $\text{Fc}/\text{Fc}^+$ .<sup>[20,81]</sup> This revealed that the HOMO energies of the bay-arylated OAPPDOs (**6a–e**) were shifted to higher energies compared to the parent compound **3a**.

A radical cation  $\text{OAPPDO}^{\bullet+}$  was generated in solution with complete conversion of the neutral precursor through the reaction of OAPPDO **3a** with one equivalent of  $\text{AgSbF}_6$  and was characterized by EPR spectroscopy (Figure 9). While hyperfine coupling to  $^{14}\text{N}$  was not detected, the observed  $g$  value of 2.003 is consistent with the value of typical organic radicals.<sup>[82]</sup>

The oxidation of compound **3a** to the corresponding radical cation was further investigated using UV/Vis spectro-electrochemistry. The sequential changes of the UV/Vis spectra during the oxidation to the radical cation are displayed in Figure 10. The spectra revealed an isosbestic point at 518 nm. The resulting radical cation upon complete oxidation was observed as a blue species with two intense absorption bands at 591 and 643 nm. The process was found to be fully reversible, and upon inversion of the voltage, reduction to the neutral species was found to take place.

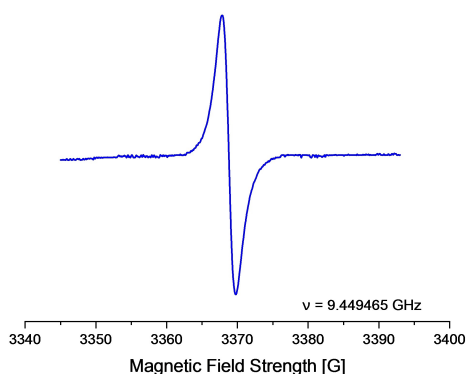


Figure 9. EPR spectrum of  $3a^{\bullet+}$  (in  $CH_2Cl_2$ , RT).

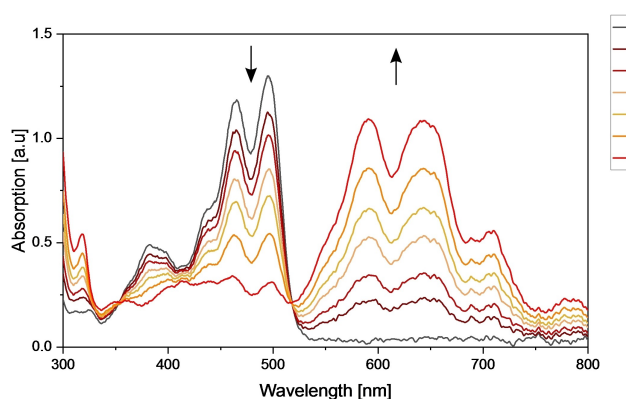


Figure 10. Series of absorption spectra of  $3a$  (in  $CH_2Cl_2$ ) during the course of electrolytic oxidation to the corresponding radical cation using TBAHFP ( $c_0 = 0.5$  M) as electrolyte and by applying a voltage of 1.4 V.

## Conclusion

In this study, we have expanded the chemistry of tetraazaperylene. With the OAPPDOs, formally derived by addition of two urea units in the opposite *peri* positions, we have established a new, highly fluorescent class of functional dyes. Even though the core has been aza-substituted four times, the electron-donating *peri* substituents favor oxidation of the aromatic core. This results in a change of redox properties compared to PDIs, rendering the OAPPDOs weak electron donors. Similar to the PDIs, substitution of the imide nitrogen atom hardly affects the optical properties and can instead be used to introduce solubility-mediating alkyl groups. As structural units, the two urea-derived *peri*-connected moieties may be viewed as structurally complementary to the dicarboximido units in the equivalent positions of the PDIs.

The synthesis of the bay-chlorinated OAPPDO  $3a$  was the key entry point for further bay functionalization, as exemplified by Suzuki coupling of various aryl fluoroborates. In contrast to OAPPDO  $3a$ , the atropisomers of its arylated derivatives are configurationally stable, as indicated by DFT modeling of the isomerization mechanism. In addition, it has been shown for one of the aryl coupled derivatives ( $6d$ ) that its atropisomers

can indeed be separated by HPLC using a chiral stationary phase. This allowed the chiroptical properties of this representative compound to be investigated. The optical and electrochemical properties of compounds  $6a$ – $e$  were fully characterized by UV/Vis and fluorescence spectroscopy as well as cyclic voltammetry. Generally, the arylation resulted in a decrease in the fluorescence quantum yields as well as in a reduction in the oxidation potentials.

Future investigations of this new class of dyes will particularly focus on their properties as emitters, both in solution and in the solid state.

## Experimental Section

**General Information:** All chemicals and solvents were purchased from commercial suppliers and used without further purification. Solvents were dried according to standard procedures. Deuterated solvents were bought from Euriso Top or Sigma–Aldrich and used as received. The  $^1H$ ,  $^{13}C$  and  $^{19}F$  spectra were recorded with Bruker AVANCE 400 and 600II spectrometers and are referenced to the residual signal of the used deuterated solvents ( $^1H$ :  $CDCl_3$ : 7.26 ppm,  $CD_2Cl_2$ : 5.32 ppm,  $[D_8]THF$ : 1.72/3.58 ppm,  $[D_6]DMSO$ : 2.50 ppm) and  $^{13}C$ :  $CDCl_3$ : 77.16 ppm,  $CH_2Cl_2$ : 53.84 ppm,  $[D_8]THF$ : 67.21/25.31 ppm,  $[D_6]DMSO$ : 39.52 ppm).<sup>[84]</sup> Chemical shifts are given in ppm and coupling constants in Hz. The following abbreviations were used to describe the multiplicities: *s* = singlet, *d* = doublet, *t* = triplet, *q* = quartet, *quint* = quintet, *m* = multiplet. The mass spectra were recorded by the department of the organic chemistry of the University of Heidelberg under the direction of Dr. J. Gross. EI spectra were measured on a JEOL JMS 700 spectrometer, ESI spectra on a Bruker ApexQe hybrid 9.4 T FT-ICR (also for MALDI spectra) or a Finnigan LCQ spectrometer. The absorption spectra were recorded on a Cary 5000 UV/Vis spectrometer and were baseline and solvent corrected. The CD spectra were recorded on a Jasco J-1500 CD spectrometer and the fluorescence spectra were recorded on a Varian Cary Eclipse Fluorescence spectrophotometer. The fluorescence yields ( $\Phi$ ) were conducted on a JASCO spectrofluorometer FP-8500 equipped with an ILF-835|100 mm integrating sphere. Cyclic voltammetry spectra were measured on a EG&G Princeton Applied Research potentiostat model 263 A using a three-electrode single-component cell under inert atmosphere. A platinum disk was used as working electrode, platinum wire as a counter electrode and a saturated calomel electrode as a reference electrode. As internal reference, ferrocene was used in all cases. Measurements were carried out in a 0.1 M tetrabutylammonium hexafluorophosphate solution in anhydrous THF under exclusion of oxygen. X-ray analyses were performed by Prof. Dr. H. Wadepohl in the X-ray laboratory of the Department of Inorganic Chemistry at the University of Heidelberg with an Agilent Supernova E diffractometer. The obtained structures were solved and refined by Prof. Dr. H. Wadepohl. Unless otherwise stated, all preparative work was performed in an inert gas atmosphere in standard Schlenk glassware, which was flame-dried.

**General Procedure 1:** Octachlorotetraazaperylene **1** (1.00 equiv.) was dissolved in *o*-xylene, the corresponding amine (20 equiv.) was added and the reaction mixture was stirred for 3 h at 140 °C. The solution was allowed to cool to RT, and the solvent was removed under reduced pressure. The residue was washed with water, methanol and *n*-pentane to isolate the corresponding tetraaminoperylene **2**.

**General Procedure 2:** Tetraaminoperylene **2** was dissolved in  $CH_2Cl_2$  and subsequently triethylamine (4.00 equiv.) and triphosgene

(1.25 equiv.) were added at  $-5^{\circ}\text{C}$ . The solution was stirred for 1 h at  $-5^{\circ}\text{C}$  and afterwards quenched with  $\text{NaOH}_{(\text{aq})}$ . The reaction mixture was extracted with  $\text{CH}_2\text{Cl}_2$ , and the solvent was removed under reduced pressure. The crude product was purified using flash column chromatography to isolate the corresponding OAPPDO 3.

**General Procedure 3:** Compound **3** (1.00 equiv.), the corresponding potassium aryltrifluoroborate (20.0 equiv.),  $\text{K}_2\text{CO}_3$  (21.0 equiv.) and 10 mol%  $\text{Pd}(\text{PPh}_3)_4$  were solved in a mixture of toluene/water/ethanol (5:2.5:1) and stirred for 3 d at  $80^{\circ}\text{C}$ . The reaction mixture was quenched with water, extracted with  $\text{CH}_2\text{Cl}_2$  and the solvent of the combined organic layers was removed under reduced pressure. The crude product was purified using flash column chromatography to isolate the corresponding chiral OAPPDO 4.

**1,3,4,6,7,9,10,12-Octachloro-2,5,8,11-tetraazaperylene (1):** 4,10-dihydroxy-5,11-dihydro-2,5,8,11-tetraazaperylene, 1,3,6,7,9,12-hexaone (2.50 g, 6.54 mmol, 1.00 equiv.),  $\text{PCl}_5$  (25.0 g, 120 mmol, 18.4 equiv.) and phosphoryl chloride (25 mL, 268 mmol, 41.0 equiv.) were stirred at  $160^{\circ}\text{C}$  for 2 d. The reaction mixture was allowed to cool down to RT and poured onto 1 L ice water. The orange precipitation was filtered and washed with 400 mL water and 50 mL methanol. The product was isolated as an orange solid (2.10 g, 3.95 mmol, 83%).  $^{13}\text{C}$  NMR (150.90 MHz,  $[\text{D}_5]$ nitrobenzene, 295 K):  $\delta = 148.3, 146.5, 144.6, 117.1, 116.9$  ppm. HRMS (MALDI $^{-}$ ): calcd. for  $\text{C}_{16}\text{Cl}_8\text{N}_4$ : 527.7637 [M] $^{-}$ ; found: 527.7642.

**1,6,7,12-Tetrachloro- $N^3, N^4, N^9, N^{10}$ -tetrahexyl-2,5,8,11-tetraazaperylene-3,4,9,10-tetraamine (2 a):** According to GP 1 1,3,4,6,7,9,10,12-octachloro-2,5,8,11-tetraazaperylene (5.00 g, 9.40 mmol, 1.00 equiv.) and hexylamine (25.0 mL, 189 mmol, 20.1 equiv.) were dissolved in 100 mL *o*-xylene and stirred at  $140^{\circ}\text{C}$  for 3 h. The reaction mixture was allowed to cool down to RT and the solvent was removed under reduced pressure. The residue was dissolved in 500 mL diethyl ether and washed with water (3x 300 mL). After removal of the solvent in vacuo, the residue was washed with *n*-pentane to obtain the product as a red solid (5.30 g, 6.70 mmol, 71%).  $^1\text{H}$  NMR (600.13 MHz,  $\text{CDCl}_3$ , 295 K):  $\delta = 5.56$  (t,  $^3J_{\text{H-H}} = 5.08$  Hz, 4H, NH), 3.60 (sext,  $^3J_{\text{H-H}} = 6.53$  Hz, 4H), 3.48 (sext,  $^3J_{\text{H-H}} = 5.21$  Hz, 4H), 1.71 (quint,  $^3J_{\text{H-H}} = 7.21$  Hz, 8H), 1.47 (quint,  $^3J_{\text{H-H}} = 7.38$  Hz, 8H), 1.36 (m, 16H), 0.91 ppm (t,  $^3J_{\text{H-H}} = 6.54$  Hz, 12H).  $^{13}\text{C}$  NMR (150.90 MHz,  $\text{CDCl}_3$ , 295 K):  $\delta = 153.1, 144.7, 144.5, 109.0, 98.5, 42.5, 31.6, 29.4, 27.1, 22.7, 14.1$  ppm. HRMS (DART $^{+}$ ): calcd. for  $\text{C}_{40}\text{H}_{56}\text{Cl}_4\text{N}_8$ : 789.3455 [M+H] $^{+}$ ; found: 789.3455.

**1,6,7,12-Tetrachloro- $N^3, N^4, N^9, N^{10}$ -tetrakis(4-methoxybenzyl)dipyrido[3,4,5-de:3',4',5'-gh][2,9]phenanthroline-3,4,9,10-tetraamine (2 b):** According to GP 1 1,3,4,6,7,9,10,12-octachloro-2,5,8,11-tetraazaperylene (10.0 g, 18.8 mmol, 1.00 equiv.) and 4-methoxy benzylamine (61.0 mL, 470 mmol, 25.0 equiv.) were dissolved in 180 mL *o*-xylene and stirred at  $140^{\circ}\text{C}$  for 3 h. After cooling down to RT the reaction mixture was poured onto 400 mL methanol and the resulting orange precipitation was filtered. The solid was washed with 200 mL water and 200 mL methanol and the solvent residues were removed under reduced pressure to yield the product as a red orange solid (13.5 g, 14.4 mmol, 77%).  $^1\text{H}$  NMR (600.13 MHz,  $\text{CDCl}_3$ , 295 K):  $\delta = 7.14$  (d,  $^3J_{\text{H-H}} = 7.95$  Hz, 8H), 6.81 (d,  $^3J_{\text{H-H}} = 8.30$  Hz, 8H), 5.79 (s, 4H, NH), 4.50–4.43 (m, 8H), 3.81 ppm (s, 12H).  $^{13}\text{C}$  NMR (150.90 MHz,  $\text{CDCl}_3$ , 295 K):  $\delta = 159.2, 152.6, 144.6, 144.0, 129.7, 129.4, 125.8, 114.2, 98.5, 55.3, 46.4$  ppm. HRMS (MALDI $^{+}$ ): calcd. for  $\text{C}_{48}\text{H}_{40}\text{Cl}_4\text{N}_4\text{O}_4$ : 932.1921 [M] $^{+}$ ; found: 932.1941.

**Compound 3a:** According to GP2 compound **2a** (5.58 g, 7.06 mmol, 1.00 equiv.) was dissolved in 100 mL  $\text{CH}_2\text{Cl}_2$  and cooled down to  $-5^{\circ}\text{C}$ . Triethyl amine (3.93 mL, 28.2 mmol, 4.00 equiv.) and triphosgene (2.62 g, 8.82 mmol, 1.25 equiv.) were added and the reaction mixture was stirred for 1 h at  $-5^{\circ}\text{C}$ . The reaction mixture was quenched with 100 mL NaOH and extracted with  $\text{CH}_2\text{Cl}_2$  (3x

100 mL). The solvent was removed under reduced pressure and the crude product was purified using flash column chromatography ( $\text{SiO}_2$ , PE/EE 20:1). The product was isolated as a yellow solid (3.10 g, 7.06 mmol, 52%).  $^1\text{H}$  NMR (600.13 MHz,  $\text{CDCl}_3$ , 295 K):  $\delta = 4.31$  (m, 4H), 4.22 (m, 4H), 1.76 (m, 8H), 1.31–1.43 (m, 24H), 0.89 ppm (t,  $^3J_{\text{H-H}} = 7.94$  Hz, 12H).  $^{13}\text{C}$  NMR (150.90 MHz,  $\text{CDCl}_3$ , 295 K):  $\delta = 150.2, 148.1, 147.7, 146.4, 112.4, 100.6, 43.1, 31.4, 27.1, 26.5, 22.6, 14.1$  ppm. HRMS (EI $^{+}$ ): calcd. for  $\text{C}_{42}\text{H}_{52}\text{Cl}_4\text{N}_8\text{O}_2$ : 840.2962 [M] $^{+}$ ; found: 840.2951.

**Compound (3b):** According to GP2 compound **2b** (1.50 g, 1.60 mmol, 1.00 equiv.) was dissolved in 100 mL  $\text{CH}_2\text{Cl}_2$  and cooled down to  $-5^{\circ}\text{C}$ . Triethyl amine (894  $\mu\text{L}$ , 6.42 mmol, 4.00 equiv.) and triphosgene (595 mg, 2.01 mmol, 1.25 equiv.) were added and the reaction mixture was stirred for 1 h at  $-5^{\circ}\text{C}$ . The reaction mixture was quenched with 100 mL NaOH and extracted with  $\text{CH}_2\text{Cl}_2$  (3x 100 mL). The solvent was removed under reduced pressure and the crude product was purified using flash column chromatography ( $\text{SiO}_2$ , PE/EE 10:1). The product was isolated as a yellow solid (1.36 g, 1.38 mmol, 86%).  $^1\text{H}$  NMR (600.13 MHz,  $\text{CDCl}_3$ , 295 K):  $\delta = 7.60$  (d,  $^3J_{\text{H-H}} = 8.69$  Hz, 8H), 6.84 (d,  $^3J_{\text{H-H}} = 8.72$  Hz, 8H), 5.38 (q,  $^3J_{\text{H-H}} = 13.94$ , 8H), 3.76 ppm (s, 12H).  $^{13}\text{C}$  NMR (150.90 MHz,  $\text{CDCl}_3$ , 295 K):  $\delta = 159.4, 150.5, 147.8, 147.5, 146.4, 131.2, 128.1, 114.0, 112.6, 100.6, 55.3, 45.4$  ppm. HRMS (EI $^{+}$ ): calcd. for  $\text{C}_{50}\text{H}_{36}\text{Cl}_4\text{N}_8\text{O}_6^{+}$ : 984.1506 [M] $^{+}$ ; found: 984.1504.

**Compound 4:** Compound **3b** (75.0 mg, 76.0  $\mu\text{mol}$ , 1.00 equiv.) was dissolved in 5 mL TFA and was stirred for 16 h at  $80^{\circ}\text{C}$ . The solvent was removed under reduced pressure and the residue was suspended in 10 mL water. The reaction mixture was neutralized with  $\text{K}_2\text{CO}_3$  and the resulting precipitate was filtered. The solid was washed with water (1x 10 mL), methanol (3x 10 mL), acetone (3x 10 mL), toluene (3x 10 mL) and *n*-pentane (3x 10 mL) to obtain the product as a yellow orange solid (28.0 mg, 55.3  $\mu\text{mol}$ , 73%).  $^1\text{H}$  NMR (600.13 MHz,  $[\text{D}_6]$ DMSO, 295 K):  $\delta = 12.2$  ppm (s, 4H, NH).  $^{13}\text{C}$  NMR (150.90 MHz,  $[\text{D}_6]$ DMSO, 295 K):  $\delta = 150.6, 150.5, 147.0, 145.6, 111.8, 100.8$  ppm. HRMS (MALDI $^{-}$ ): calcd. for  $\text{C}_{18}\text{H}_3\text{Cl}_4\text{N}_8\text{O}_2^{-}$ : 502.9139 [M-H] $^{-}$ ; found: 502.9143.

**Compound 5:** Compound **3a** (100 mg, 119  $\mu\text{mol}$ , 1.00 equiv.) was dissolved in 15 mL THF and  $\text{Pd}(\text{dppf})\text{Cl}_2$  (26.0 mg, 35.7  $\mu\text{mol}$ , 30 mol%), TMEDA (250  $\mu\text{L}$ , 1.66 mmol, 14.0 equiv.) and sodium borohydride (62.9 mg, 1.66 mmol, 14.0 equiv.) were added. The reaction mixture was stirred for 2 d at  $65^{\circ}\text{C}$ , poured onto 50 mL water and extracted with  $\text{CH}_2\text{Cl}_2$  (3x 100 mL). The solvent was removed and the crude product was purified using flash column chromatography ( $\text{SiO}_2$ , PE/EE 5:1). The product was isolated as a yellow solid (26.0 mg, 36.9  $\mu\text{mol}$ , 31%).  $^1\text{H}$  NMR (600.13 MHz,  $\text{CDCl}_3$ , 295 K):  $\delta = 8.47$  (s, 4H), 4.17 (t,  $^3J_{\text{H-H}} = 7.03$  Hz, 8H), 1.70 (quint,  $^3J_{\text{H-H}} = 6.35$  Hz, 8H), 1.40 (m, 8H), 1.35–1.30 (m, 16H), 0.88 ppm (t,  $^3J_{\text{H-H}} = 6.55$  Hz, 12H).  $^{13}\text{C}$  NMR (150.90 MHz,  $\text{CDCl}_3$ , 295 K):  $\delta = 150.5, 149.2, 139.4, 137.1, 115.7, 104.0, 42.5, 31.6, 27.2, 26.7, 22.7, 14.1$  ppm. HRMS (EI $^{+}$ ): calcd. for  $\text{C}_{42}\text{H}_{56}\text{N}_8\text{O}_2$ : 704.4521 [M] $^{+}$ ; found: 704.4519.

**Compound 6a:** According to GP3 compound **3a** (100 mg, 119  $\mu\text{mol}$ , 1.00 equiv.), potassium phenyltrifluoroborate (437 mg, 2.37 mmol, 20.0 equiv.),  $\text{K}_2\text{CO}_3$  (344 mg, 2.49 mmol, 21.0 equiv.) and  $\text{Pd}(\text{PPh}_3)_4$  (13.7 mg, 11.9  $\mu\text{mol}$ , 10 mol%) were dissolved in a mixture of 10 mL toluene, 5 mL water and 2 mL ethanol and stirred for 3 d at  $80^{\circ}\text{C}$ . The reaction mixture was allowed to cool down to RT, quenched with 20 mL water and extracted with  $\text{CH}_2\text{Cl}_2$  (3x 100 mL). The solvent was removed under reduced pressure and the residue was purified using flash column chromatography ( $\text{SiO}_2$ , PE/EE 30:1). The product was isolated as a red solid (63.0 mg, 62.4  $\mu\text{mol}$ , 53%).  $^1\text{H}$  NMR (600.13 MHz,  $\text{CDCl}_3$ , 295 K):  $\delta = 7.24$  (t,  $^3J_{\text{H-H}} = 7.51$  Hz, 4H), 7.20–7.04 (brs, 8H), 7.12 (t,  $^3J_{\text{H-H}} = 7.29$  Hz, 8H), 4.47–4.43 (m, 4H), 4.36–4.31 (m, 4H), 1.85 (quint,  $^3J_{\text{H-H}} = 7.29$  Hz, 8H),

1.51–1.40 (m, 24H), 0.98 ppm (t,  $^3J_{\text{H-H}}=6.88$  Hz, 12H).  $^{13}\text{C}$  NMR (150.90 MHz,  $\text{CDCl}_3$ , 295 K):  $\delta=154.9$ , 151.2, 147.9, 145.4, 141.1, 128.4, 128.2, 128.0, 114.4, 101.3, 42.1, 31.7, 27.4, 26.7, 22.7, 14.0 ppm. HRMS (EI $^+$ ): calcd for  $\text{C}_{66}\text{H}_{72}\text{N}_8\text{O}_2$ : 1008.5773 [M] $^+$ ; found: 1008.5762.

**Compound 6b:** According to GP3 compound **3a** (150 mg, 178  $\mu\text{mol}$ , 1.00 equiv.), potassium 4-methylphenyltrifluoroborate (705 mg, 3.56 mmol, 20.0 equiv.),  $\text{K}_2\text{CO}_3$  (517 mg, 3.74 mmol, 21.0 equiv.) and  $\text{Pd}(\text{PPh}_3)_4$  (20.6 mg, 17.8  $\mu\text{mol}$ , 10 mol%) were dissolved in a mixture of 15 mL toluene, 7.5 mL water and 3 mL ethanol and stirred for 3 d at 80°C. The reaction mixture was allowed to cool down to RT, quenched with 20 mL water and extracted with  $\text{CH}_2\text{Cl}_2$  (3x 100 mL). The solvent was removed under reduced pressure and the residue was purified using flash column chromatography ( $\text{SiO}_2$ , PE/EE 20:1). The product was isolated as a red solid (83.0 mg, 80.3  $\mu\text{mol}$ , 45%).  $^1\text{H}$  NMR (600.13 MHz,  $\text{CDCl}_3$ , 295 K):  $\delta=7.19$  (d,  $^3J_{\text{H-H}}=4.40$  Hz, 8H), 6.74 (t,  $^3J_{\text{H-H}}=4.34$  Hz, 8H), 4.33 (m, 4H), 4.25 (m, 4H), 1.79 (quint,  $^3J_{\text{H-H}}=7.73$  Hz, 8H), 1.45–1.41 (m, 8H), 1.37–1.30 (m, 16H), 0.88 ppm (t,  $^3J_{\text{H-H}}=7.11$  Hz, 12H).  $^{13}\text{C}$  NMR (150.90 MHz,  $\text{CDCl}_3$ , 295 K):  $\delta=151.0$ , 147.7, 147.3, 146.1, 145.0, 128.5, 127.4, 126.2, 113.1, 100.8, 42.6, 31.6, 27.2, 26.7, 22.7, 14.1 ppm. HRMS (MALDI $^+$ ): calcd. for  $\text{C}_{58}\text{H}_{64}\text{N}_8\text{O}_2\text{S}_4$ : 1032.4030 [M] $^+$ ; found: 1032.4024.

**Compound 6c:** According to GP3 compound **3a** (150 mg, 178  $\mu\text{mol}$ , 1.00 equiv.), potassium 4-methoxyphenyltrifluoroborate (762 mg, 3.56 mmol, 20.0 equiv.),  $\text{K}_2\text{CO}_3$  (517 mg, 3.74 mmol, 21.0 equiv.) and  $\text{Pd}(\text{PPh}_3)_4$  (20.6 mg, 17.8  $\mu\text{mol}$ , 10 mol%) were dissolved in a mixture of 15 mL toluene, 7.5 mL water and 3 mL ethanol and stirred for 3 d at 80°C. The reaction mixture was allowed to cool down to RT, quenched with 20 mL water and extracted with  $\text{CH}_2\text{Cl}_2$  (3x 100 mL). The solvent was removed under reduced pressure and the residue was purified using flash column chromatography ( $\text{SiO}_2$ , PE/EE 30:1). The product was isolated as a red solid (95.0 mg, 84.1  $\mu\text{mol}$ , 47%).  $^1\text{H}$  NMR (600.13 MHz,  $\text{CDCl}_3$ , 295 K):  $\delta=7.06$  (brs, 8H), 6.57 (d,  $^3J_{\text{H-H}}=8.62$  Hz, 8H), 4.34–4.30 (m, 4H), 4.24–4.19 (m, 4H), 3.79 (s, 12H), 1.74 (quint,  $^3J_{\text{H-H}}=7.34$  Hz, 8H), 1.40–1.29 (m, 24H), 0.88 ppm (t,  $^3J_{\text{H-H}}=7.17$  Hz, 12H).  $^{13}\text{C}$  NMR (150.90 MHz,  $\text{CDCl}_3$ , 295 K):  $\delta=159.6$ , 154.2, 151.3, 147.4, 145.6, 133.9, 129.7, 114.0, 113.6, 100.9, 55.4, 42.1, 31.6, 27.3, 26.6, 22.6, 14.1 ppm. HRMS (MALDI $^+$ ): calcd. for  $\text{C}_{70}\text{H}_{80}\text{N}_8\text{O}_6$ : 1128.6195 [M] $^+$ ; found: 1128.6199.

**Compound 6d:** According to GP3 compound **3a** (150 mg, 178  $\mu\text{mol}$ , 1.00 equiv.), potassium 4-trifluoromethylphenyltrifluoroborate (659 mg, 3.56 mmol, 20.0 equiv.),  $\text{K}_2\text{CO}_3$  (517 mg, 3.74 mmol, 21.0 equiv.) and  $\text{Pd}(\text{PPh}_3)_4$  (20.6 mg, 17.8  $\mu\text{mol}$ , 10 mol%) were dissolved in a mixture of 15 mL toluene, 7.5 mL water and 3 mL ethanol and stirred for 3 d at 80°C. The reaction mixture was allowed to cool down to RT, quenched with 20 mL water and extracted with  $\text{CH}_2\text{Cl}_2$  (3x 100 mL). The solvent was removed under reduced pressure and the residue was purified using flash column chromatography ( $\text{SiO}_2$ , PE/EE 25:1). The product was isolated as a red solid (101 mg, 78.8  $\mu\text{mol}$ , 44%).  $^1\text{H}$  NMR (600.13 MHz,  $\text{CDCl}_3$ , 295 K):  $\delta=7.29$  (d,  $^3J_{\text{H-H}}=8.07$  Hz, 8H), 7.10 (brs, 8H), 4.29 (m, 8H), 1.74 (quint,  $^3J_{\text{H-H}}=7.44$  Hz, 8H), 1.44–1.26 (m, 24H), 0.86 ppm (t,  $^3J_{\text{H-H}}=7.12$  Hz, 12H).  $^{19}\text{F}$  NMR (379.27 MHz,  $\text{CDCl}_3$ , 295 K):  $\delta=-63.0$  ppm (s, 12F).  $^{13}\text{C}$  NMR (150.90 MHz,  $\text{CDCl}_3$ , 295 K):  $\delta=153.7$ , 150.7, 148.2, 145.1, 143.9, 130.0 (q,  $^2J_{\text{C-F}}=32.4$  Hz), 124.0 (q,  $^1J_{\text{C-F}}=271.1$  Hz,  $\text{CF}_3$ ), 114.1, 101.6, 42.6, 31.5, 27.2, 26.6, 22.5, 14.0 ppm. HRMS (MALDI $^+$ ): calcd. for  $\text{C}_{70}\text{H}_{68}\text{F}_{12}\text{N}_8\text{O}_2$ : 1280.5628 [M] $^+$ ; found: 1280.5299.

**Compound 6e:** According to GP3 compound **3a** (150 mg, 178  $\mu\text{mol}$ , 1.00 equiv.), potassium 2-thiophenyltrifluoroborate (676 mg, 3.56 mmol, 20.0 equiv.),  $\text{K}_2\text{CO}_3$  (517 mg, 3.74 mmol, 21.0 equiv.) and  $\text{Pd}(\text{PPh}_3)_4$  (20.6 mg, 17.8  $\mu\text{mol}$ , 10 mol%) were dissolved in a mixture of 15 mL toluene, 7.5 mL water and 3 mL

ethanol and stirred for 3 d at 80°C. The reaction mixture was allowed to cool down to RT, quenched with 20 mL water and extracted with  $\text{CH}_2\text{Cl}_2$  (3x 100 mL). The solvent was removed under reduced pressure and the residue was purified using flash column chromatography ( $\text{SiO}_2$ , PE/EE 20:1). The product was isolated as a red purple solid (83.0 mg, 80.3  $\mu\text{mol}$ , 45%).  $^1\text{H}$  NMR (600.13 MHz,  $\text{CDCl}_3$ , 295 K):  $\delta=7.19$  (d,  $^3J_{\text{H-H}}=4.40$  Hz, 8H), 6.74 (t,  $^3J_{\text{H-H}}=4.34$  Hz, 8H), 4.33 (m, 4H), 4.25 (m, 4H), 1.79 (quint,  $^3J_{\text{H-H}}=7.73$  Hz, 8H), 1.45–1.41 (m, 8H), 1.37–1.30 (m, 16H), 0.88 ppm (t,  $^3J_{\text{H-H}}=7.11$  Hz, 12H).  $^{13}\text{C}$  NMR (150.90 MHz,  $\text{CDCl}_3$ , 295 K):  $\delta=151.0$ , 147.7, 147.3, 146.1, 145.0, 128.5, 127.4, 126.2, 113.1, 100.8, 42.6, 31.6, 27.2, 26.7, 22.7, 14.1 ppm. HRMS (MALDI $^+$ ): calcd. for  $\text{C}_{58}\text{H}_{64}\text{N}_8\text{O}_2\text{S}_4$ : 1032.4030 [M] $^+$ ; found: 1032.4024.

**Compound 7:** Compound **3a** (150 mg, 178  $\mu\text{mol}$ , 1.00 equiv.), tributylphenylstannane (128  $\mu\text{L}$ , 392  $\mu\text{mol}$ , 2.20 equiv.) and  $\text{Pd}(\text{PPh}_3)_4$  (41.1 mg, 35.6  $\mu\text{mol}$ , 20 mol%) were dissolved in 5 mL toluene and stirred for 2 d at 110°C. The reaction mixture was allowed to cool down to RT, poured onto 100 mL water and extracted with  $\text{CH}_2\text{Cl}_2$  (3x 100 mL). The solvent was removed under reduced pressure and the crude product was purified using flash column chromatography ( $\text{SiO}_2$ , PE/EE 3:1). The product was isolated as a yellow solid (28.0 mg, 33.0  $\mu\text{mol}$ , 19%).  $^1\text{H}$  NMR (600.13 MHz,  $\text{CD}_2\text{Cl}_2$ , 295 K):  $\delta=8.33$  (brs, 2H), 7.28 (brs, 2H), 4.17 (brs, 8H), 1.85 (brs, 4H), 1.74 (quint,  $^3J_{\text{H-H}}=6.91$  Hz, 4H), 1.53–1.35 (m, 24H), 0.98 (t,  $^3J_{\text{H-H}}=7.06$  Hz, 6H), 0.94 ppm (t,  $^3J_{\text{H-H}}=7.02$  Hz, 6H).  $^{13}\text{C}$  NMR (150.90 MHz,  $\text{CD}_2\text{Cl}_2$ , 295 K):  $\delta=150.4$ , 147.7, 147.6, 146.9, 139.6, 138.3, 130.2, 127.5, 124.0, 112.9, 109.6, 99.8, 42.8, 42.5, 31.6, 31.5, 27.2, 26.9, 26.8, 26.6, 22.7, 22.7, 13.9 ppm. HRMS (MALDI $^+$ ): calcd. for  $\text{C}_{48}\text{H}_{56}\text{Cl}_2\text{N}_8\text{O}_2$ : 846.3898 [M] $^+$ ; found: 846.3902.

**Compound 8:** Compound **3a** (262 mg, 311  $\mu\text{mol}$ , 1.00 equiv.), potassium phenyltrifluoroborate (120 mg, 652  $\mu\text{mol}$ , 2.10 equiv.),  $\text{K}_2\text{CO}_3$  (858 mg, 6.21 mmol, 20.0 equiv.) and  $\text{Pd}(\text{PPh}_3)_4$  (53.8 mg, 46.6  $\mu\text{mol}$ , 15 mol%) were dissolved in a mixture of 17 mL toluene, 8 mL water and 3.5 mL ethanol and stirred for 3 d at 80°C. The reaction mixture was allowed to cool down to RT, quenched with 20 mL water and extracted with  $\text{CH}_2\text{Cl}_2$  (3x 100 mL). The solvent was removed under reduced pressure and the residue was purified using flash column chromatography ( $\text{SiO}_2$ , PE/EE 25:1). The product was isolated as a yellow solid (23.0 mg, 26.9  $\mu\text{mol}$ , 9%).  $^1\text{H}$  NMR (600.13 MHz,  $\text{CD}_2\text{Cl}_2$ , 295 K):  $\delta=8.85$  (d,  $^3J_{\text{H-H}}=7.48$  Hz, 1H), 8.76 (d,  $^3J_{\text{H-H}}=7.58$  Hz, 1H), 7.95 (s, 1H), 7.68–7.64 (m, 2H), 7.63 (brs, 5H), 4.35 (t,  $^3J_{\text{H-H}}=7.91$  Hz, 2H), 4.27–4.22 (m, 4H), 4.14 (t,  $^3J_{\text{H-H}}=7.77$  Hz, 2H), 1.85 (quint,  $^3J_{\text{H-H}}=7.43$  Hz, 2H), 1.82–1.75 (m, 4H), 1.68 (quint,  $^3J_{\text{H-H}}=7.07$  Hz, 2H), 1.51–1.28 (m, 24H), 0.96–0.86 ppm (m, 12H).  $^{13}\text{C}$  NMR (150.90 MHz,  $\text{CD}_2\text{Cl}_2$ , 295 K):  $\delta=155.1$ , 151.0, 150.8, 148.4, 148.2, 147.6, 147.4, 146.9, 146.1, 142.6, 139.8, 139.3, 136.6, 135.5, 130.1, 130.4, 129.8, 129.2, 128.4, 127.7, 127.6, 124.3, 124.1, 116.2, 113.5, 111.2, 110.8, 101.8, 101.2, 42.5, 42.5, 42.2, 42.2, 31.8, 31.8, 31.8, 31.6, 27.4, 27.3, 27.0, 27.0, 27.0, 26.9, 26.7, 26.7, 22.9, 22.9, 22.8, 22.7, 14.1, 14.1, 14.0, 14.0 ppm. HRMS (MALDI $^+$ ): calcd. for  $\text{C}_{54}\text{H}_{62}\text{N}_8\text{O}_2$ : 854.4999 [M] $^+$ ; found: 854.4988.

Deposition Numbers 2154823 (for **6a**), 2154824 (for **6b**), 2154825 (for **6c**) and 2154826 (for **6d**) contain the supplementary crystallographic data for this paper. These data are provided free of charge by the joint Cambridge Crystallographic Data Centre and Fachinformationszentrum Karlsruhe Access Structures service.

## Acknowledgements

The authors acknowledge support by the state of Baden-Württemberg through bwHPC and the German Research Foundation (DFG) through no. INST40/467-1FUGG (Justus

cluster) and thank the DFG for funding within the framework of SFB1249 (TP A2). We also thank Tobias Kirschbaum and Prof Michael Mastalerz for access to their CD spectroscopy equipment. Open Access funding enabled and organized by Projekt DEAL.

## Conflict of Interest

The authors declare no conflict of interest.

## Data Availability Statement

The data that support the findings of this study are available in the supplementary material of this article.

**Keywords:** azaperylenes · density functional calculations · fluorescence · N-heteropolycycles · organic dyes

- [1] K. Hunger, W. Herbst, *Ullmann's Encyclopedia of Industrial Chemistry*, Wiley-VCH, Weinheim, **2000**, pp. 379–423.
- [2] F. Würthner, *Chem. Commun.* **2004**, 1564–1579.
- [3] G. Seybold, G. Wagenblast, *Dyes Pigment.* **1989**, *11*, 303–317.
- [4] F. Würthner, C. R. Saha-Möller, B. Fimmel, S. Ogi, P. Leowanawat, D. Schmidt, *Chem. Rev.* **2016**, *116*, 962–1052.
- [5] A. Nowak-Król, F. Würthner, *Org. Chem. Front.* **2019**, *6*, 1272–1318.
- [6] W. Herbst, K. Hunger, *Industrial Organic Pigments*, 3rd, rev. ed., Wiley-VCH, Weinheim, **2004**.
- [7] H. Langhals, S. Demmig, H. Huber, *Spectrochim. Acta Part A* **1988**, *44*, 1189–1193.
- [8] M. Sadrai, L. Hadel, R. R. Sauers, S. Husain, K. Krogh-Jespersen, J. D. Westbrook, G. R. Bird, *J. Phys. Chem.* **1992**, *96*, 7988–7996.
- [9] U. Rohr, P. Schlichting, A. Böhm, M. Gross, K. Meerholz, C. Bräuchle, K. Müllen, *Angew. Chem. Int. Ed.* **1998**, *37*, 1434–1437; *Angew. Chem.* **1998**, *110*, 1463–1467.
- [10] M. J. Ahrens, M. J. Fuller, M. R. Wasielewski, *Chem. Mater.* **2003**, *15*, 2684–2686.
- [11] Y. Zhao, M. R. Wasielewski, *Tetrahedron Lett.* **1999**, *40*, 7047–7050.
- [12] H. Langhals, S. Demmig, T. Potrawa, *J. Prakt. Chem.* **1991**, *333*, 733–748.
- [13] C. Yan, S. Barlow, Z. Wang, H. Yan, A. K. Y. Jen, S. R. Marder, X. Zhan, *Nat. Rev. Mater.* **2018**, *3*, 18003.
- [14] C. Huang, S. Barlow, S. R. Marder, *J. Org. Chem.* **2011**, *76*, 2386–2407.
- [15] R. Jiang, Z. Xue, Y. Li, Z. Qin, Y. Li, D. Zhu, *Eur. J. Org. Chem.* **2014**, *2014*, 5004–5009.
- [16] X. Zhan, A. Facchetti, S. Barlow, T. J. Marks, M. A. Ratner, M. R. Wasielewski, S. R. Marder, *Adv. Mater.* **2011**, *23*, 268–284.
- [17] C. Li, H. Wonneberger, *Adv. Mater.* **2012**, *24*, 613–636.
- [18] W. Jiang, Y. Li, Z. Wang, *Acc. Chem. Res.* **2014**, *47*, 3135–3147.
- [19] N. Soh, T. Ueda, *Talanta* **2011**, *85*, 1233–1237.
- [20] A. Nowak-Król, K. Shoyama, M. Stolte, F. Würthner, *Chem. Commun.* **2018**, *54*, 13763–13772.
- [21] J. E. Anthony, A. Facchetti, M. Heeney, S. R. Marder, X. Zhan, *Adv. Mater.* **2010**, *22*, 3876–3892.
- [22] R. J. Chesterfield, J. C. McKeen, C. R. Newman, P. C. Ewbank, D. A. da Silva Filho, J.-L. Brédas, L. L. Miller, K. R. Mann, C. D. Frisbie, *J. Phys. Chem. B* **2004**, *108*, 19281–19292.
- [23] F.-C. Chen, C.-H. Liao, *Appl. Phys. Lett.* **2008**, *93*, 103310.
- [24] R. Schmidt, J. H. Oh, Y.-S. Sun, M. Deppisch, A.-M. Krause, K. Radacki, H. Braunschweig, M. Könemann, P. Erk, Z. Bao, F. Würthner, *J. Am. Chem. Soc.* **2009**, *131*, 6215–6228.
- [25] P. R. L. Malenfant, C. D. Dimitrakopoulos, J. D. Gelorme, L. L. Kosbar, T. O. Graham, A. Curioni, W. Andreoni, *Appl. Phys. Lett.* **2002**, *80*, 2517–2519.
- [26] T. Riehm, G. De Paoli, A. E. Konradsson, L. De Cola, H. Wadepohl, L. H. Gade, *Chem. Eur. J.* **2007**, *13*, 7317–7329.
- [27] M. Matena, T. Riehm, M. Stöhr, T. A. Jung, L. H. Gade, *Angew. Chem. Int. Ed.* **2008**, *47*, 2414–2417; *Angew. Chem.* **2008**, *120*, 2448–2451.
- [28] S. Blankenburg, E. Rauls, W. G. Schmidt, *J. Phys. Chem. Lett.* **2010**, *1*, 3266–3270.
- [29] M. Matena, M. Stöhr, T. Riehm, J. Björk, S. Martens, M. S. Dyer, M. Persson, J. Lobo-Checa, K. Müller, M. Enache, H. Wadepohl, J. Zegenhagen, T. A. Jung, L. H. Gade, *Chem. Eur. J.* **2010**, *16*, 2079–2091.
- [30] S. C. Martens, U. Zschieschang, H. Wadepohl, H. Klauk, L. H. Gade, *Chem. Eur. J.* **2012**, *18*, 3498–3509.
- [31] S. Geib, S. C. Martens, M. Märken, A. Rybina, H. Wadepohl, L. H. Gade, *Chem. Eur. J.* **2013**, *19*, 13811–13822.
- [32] L. Hahn, S. Öz, H. Wadepohl, L. H. Gade, *Chem. Commun.* **2014**, *50*, 4941–4943.
- [33] S. Höfener, B. A. R. Günther, M. E. Harding, L. H. Gade, *J. Phys. Chem. A* **2019**, *123*, 3160–3169.
- [34] B. A. R. Günther, S. Höfener, U. Zschieschang, H. Wadepohl, H. Klauk, L. H. Gade, *Chem. Eur. J.* **2019**, *25*, 14669–14678.
- [35] B. A. R. Günther, S. Höfener, R. Eichelmann, U. Zschieschang, H. Wadepohl, H. Klauk, L. H. Gade, *Org. Lett.* **2020**, *22*, 2298–2302.
- [36] S. Geib, U. Zschieschang, M. Gsänger, M. Stolte, F. Würthner, H. Wadepohl, H. Klauk, L. H. Gade, *Adv. Funct. Mater.* **2013**, *23*, 3866–3874.
- [37] Q. Ye, C. Chi, *Chem. Mater.* **2014**, *26*, 4046–4056.
- [38] M. Winkler, K. N. Houk, *J. Am. Chem. Soc.* **2007**, *129*, 1805–1815.
- [39] T. Okamoto, S. Kumagai, E. Fukuzaki, H. Ishii, G. Watanabe, N. Niitsu, T. Annaka, M. Yamagishi, Y. Tani, H. Sugiura, T. Watanabe, S. Watanabe, J. Takeya, *Sci. Adv.* **2020**, *6*, eaz0632.
- [40] E. Baal, M. Klein, K. Harms, J. Sundermeyer, *Chem. Eur. J.* **2021**, *27*, 12610–12618.
- [41] J. A. Schneider, D. F. Peregichka, *J. Mater. Chem. C* **2016**, *4*, 7269–7276.
- [42] A. Hirono, H. Sakai, S. Kochi, T. Sato, T. Hasobe, *J. Phys. Chem. B* **2020**, *124*, 9921–9930.
- [43] T. Wesp, T. Bruckhoff, J. Petry, H. Wadepohl, L. H. Gade, *Chem. Eur. J.* **2022**, *28*, e202200129.
- [44] T. Zhang, Y. Zagranyski, A. Skabeev, K. Müllen, C. Li, *Dyes Pigment.* **2021**, *196*, 109780.
- [45] M. Gsänger, D. Bialas, L. Huang, M. Stolte, F. Würthner, *Adv. Mater.* **2016**, *28*, 3615–3645.
- [46] M. Gsänger, J. H. Oh, M. Könemann, H. W. Höffken, A.-M. Krause, Z. Bao, F. Würthner, *Angew. Chem. Int. Ed.* **2010**, *49*, 740–743; *Angew. Chem.* **2010**, *122*, 752–755.
- [47] M. Irimia-Vladu, E. D. Glowacki, P. A. Troshin, G. Schwabegger, L. Leonat, D. K. Susarova, O. Krystal, M. Ullah, Y. Kanbur, M. A. Bodea, V. F. Razumov, H. Sitter, S. Bauer, N. S. Sariciftci, *Adv. Mater.* **2012**, *24*, 375–380.
- [48] H. Höchstetter (Bayer AG), DE3942893 A1, **1991**.
- [49] P. Osswald, F. Würthner, *J. Am. Chem. Soc.* **2007**, *129*, 14319–14326.
- [50] T. W. Greene, P. G. Wuts, *Protective Groups in Organic Synthesis*, Wiley-Interscience, Weinheim, **1999**.
- [51] M. Queste, C. Cadiou, B. Pagoaga, L. Giraudet, N. Hoffmann, *New J. Chem.* **2010**, *34*, 2537–2545.
- [52] W. Qiu, S. Chen, X. Sun, Y. Liu, D. Zhu, *Org. Lett.* **2006**, *8*, 867–870.
- [53] R. Renner, B. Mahlmeister, O. Anhalt, M. Stolte, F. Würthner, *Chem. Eur. J.* **2021**, *27*, 11997–12006.
- [54] S. Cacchi, P. G. Ciattini, E. Morera, G. Ortar, *Tetrahedron Lett.* **1986**, *27*, 5541–5544.
- [55] B. Pagoaga, L. Giraudet, N. Hoffmann, *Eur. J. Org. Chem.* **2014**, *2014*, 5178–5195.
- [56] L. Hahn, A. Hermannsdorfer, B. Günther, T. Wesp, B. Bühler, U. Zschieschang, H. Wadepohl, H. Klauk, L. H. Gade, *J. Org. Chem.* **2017**, *82*, 12492–12502.
- [57] P. Osswald, M. Reichert, G. Bringmann, F. Würthner, *J. Org. Chem.* **2007**, *72*, 3403–3411.
- [58] Z. Xie, F. Würthner, *Org. Lett.* **2010**, *12*, 3204–3207.
- [59] L. Zhang, S. Chen, J. Jiang, X. Dong, Y. Cai, H.-J. Zhang, J. Lin, Y.-B. Jiang, *Org. Lett.* **2022**, *24*, 3179–3183.
- [60] C. Lee, W. Yang, R. G. Parr, *Phys. Rev. B* **1988**, *37*, 785–789.
- [61] A. D. Becke, *J. Chem. Phys.* **1993**, *98*, 5648–5652.
- [62] P. J. Stephens, F. J. Devlin, C. F. Chabalowski, M. J. Frisch, *J. Phys. Chem.* **1994**, *98*, 11623–11627.
- [63] F. Weigend, R. Ahlrichs, *Phys. Chem. Chem. Phys.* **2005**, *7*, 3297–3305.
- [64] F. Weigend, *Phys. Chem. Chem. Phys.* **2006**, *8*, 1057–1065.
- [65] S. Grimme, J. Antony, S. Ehrlich, H. Krieg, *J. Chem. Phys.* **2010**, *132*, 154104.
- [66] S. Grimme, S. Ehrlich, L. Goerigk, *J. Comput. Chem.* **2011**, *32*, 1456–1465.
- [67] R. Renner, *Z. Phys.* **1934**, *92*, 172–193.
- [68] G. Herzberg, E. Teller, *Z. Phys. Chem.* **1933**, *21B*, 410–446.

- [69] H. J. Kupka, *Transitions in Molecular Systems*, Wiley-VCH, Weinheim, **2011**.
- [70] G. H. Atkinson, C. S. Parmenter, *J. Mol. Spectrosc.* **1978**, *73*, 52–95.
- [71] K. Gustav, M. Storch, *Monatsh. Chem.* **1992**, *123*, 59–62.
- [72] F. J. Avila Ferrer, V. Barone, C. Cappelli, F. Santoro, *J. Chem. Theory Comput.* **2013**, *9*, 3597–3611.
- [73] I. Benkyi, E. Tapavicza, H. Fliegl, D. Sundholm, *Phys. Chem. Chem. Phys.* **2019**, *21*, 21094–21103.
- [74] F. Neese, F. Wennmo, U. Becker, C. Riplinger, *J. Chem. Phys.* **2020**, *152*, 224108.
- [75] P. Badoz, *Optical Rotatory Dispersion and Circular Dichroism in Organic Chemistry: Including Applications from Inorganic Chemistry and Biochemistry; Proceedings of Nato Summer School Held at Bonn, 24 September-1 October, 1965*, Heyden, **1967**.
- [76] N. Berova, P. L. Polavarapu, K. Nakanishi, R. W. Woody, *Comprehensive Chiroptical Spectroscopy: Applications in Stereochemical Analysis of Synthetic Compounds, Natural Products, and Biomolecules*, Vol. 2, Wiley, **2012**.
- [77] N. Berova, P. L. Polavarapu, K. Nakanishi, R. W. Woody, *Comprehensive Chiroptical Spectroscopy: Instrumentation, Methodologies, and Theoretical Simulations*, Vol. 1, Wiley, **2011**.
- [78] M. M. Safont-Sempere, P. Osswald, K. Radacki, F. Würthner, *Chem. Eur. J.* **2010**, *16*, 7380–7384.
- [79] V. Barone, M. Cossi, *J. Phys. Chem. A* **1998**, *102*, 1995–2001.
- [80] M. Cossi, N. Rega, G. Scalmani, V. Barone, *J. Comput. Chem.* **2003**, *24*, 669–681.
- [81] C. M. Cardona, W. Li, A. E. Kaifer, D. Stockdale, G. C. Bazan, *Adv. Mater.* **2011**, *23*, 2367–2371.
- [82] S. Stoll, *Electron Paramagnetic Resonance: Vol. 22*, The Royal Society of Chemistry, **2011**, pp. 107–154.
- [83] A. Dittmer, R. Izsák, F. Neese, D. Maganas, *Inorg. Chem.* **2019**, *58*, 9303–9315.
- [84] G. R. Fulmer, A. J. M. Miller, N. H. Sherden, H. E. Gottlieb, A. Nudelman, B. M. Stoltz, J. E. Bercaw, K. I. Goldberg, *Organometallics* **2010**, *29*, 2176–2179.

---

Manuscript received: June 2, 2022

Accepted manuscript online: June 27, 2022

Version of record online: July 29, 2022